Heliyon 10 (2024) e39081

Contents lists available at ScienceDirect

Heliyon

journal homepage: www.cell.com/heliyon

Research article

Upconversion enhancement and temperature sensing studies in Li^+ ions incorporated $GdPO_4:Tm^{3+}/Yb^{3+}$ phosphor

Madan M. Upadhyay, Kaushal Kumar *

Optical Materials & Bio-imaging Research Laboratory, Department of Physics, Indian Institute of Technology (Indian School of Mines), Dhanbad, 826004, India

ARTICLE INFO

Keywords:
Lanthanides
Photon upconversion
Optical temperature sensing
Anti-counterfeiting
Non-thermally coupled levels

ABSTRACT

The $GdPO_4:Tm^{3+}/Yb^{3+}$ phosphor codoped with various concentrations of Li^+ ions were synthesized for upconversion emission and optical thermometry studies. Excitation using 980 nm laser diode results in three upconversion (UC) emission bands with centre wavelengths of 478, 648 and 692 nm. These bands are originated from $^1G_4 \rightarrow {}^3H_6$, $^1G_4 \rightarrow {}^3F_4$, and $^3F_3 \rightarrow {}^3H_6$ transitions of the Tm^{3+} ion, respectively. Li^+ ions modified the local crystal symmetry around dopant ions, resulting enhanced UC emissions. The lifetime of the $^1G_4$ level of Tm^{3+} ion was studied using a 980 nm laser excitation. The temperature sensing performances of $GdPO_4:Tm^{3+}/Yb^{3+}$ and $GdPO_4:Tm^{3+}/Yb^{3+}/Li^+$ based on fluorescence intensity ratio (FIR) technique were evaluated in the temperature range 301–713 K under 980 nm excitation. Non-thermally coupled levels $^3F_3$ (692 nm) and $^1G_4$ (478, 648 nm) were utilized for FIR estimation. A maximum absolute sensitivity of 6.28×10^{-3} K^{-1} at 653 K and 18.71×10^{-3} K^{-1} at 713 K were observed for Li^+ undoped and codoped phosphors respectively. The result indicates that codoping of Li^+ ions improved the UC emission as well as optical thermometry. Moreover, CIE colour coordinates and anti-counterfeiting application were also exhibited.

1. Introduction

Trivalent rare-earth doped upconversion (UC) luminescent materials have received considerable attention over the past few decades owing to their potential applications in areas such as temperature sensing, photovoltaic solar cells, bio-imaging, security markers, colour displays and LEDs [1–5]. The term upconversion refers to nonlinear optical processes that involve the sequential absorption of two or more low energy pump photons through intermediate long-lived energy states of rare earth ions and the subsequent emission of higher energy photons [6,7]. In practise, UC materials with high luminescence efficiency and consistent temperature sensing abilities may be desirable [8]. However, UC materials with high efficiency and excellent temperature sensitivity are rare. To achieve these criteria, it is essential to investigate new kinds of UC material. The UC efficiency is, in fact, closely linked to the phonon energy of host materials [9]. Generally, lower the phonon energy of the host material, greater the UC efficiency. Since, low lattice phonon energy minimizes non-radiative loss while increasing radiative emission [10]. Studies related to UC luminescent materials mostly centred on the formation of fluoride crystals, which have been shown to be the most effective host materials because of their relatively low phonon energy [11]. However, their uses remain severely limited due to poor thermal stability and chemical durability [12]. Oxide compounds are an appropriate type of matrix material due to their excellent chemical stability and environment

* Corresponding author.
E-mail address: kkumar@iitism.ac.in (K. Kumar).

https://doi.org/10.1016/j.heliyon.2024.e39081
Received 9 April 2024; Received in revised form 29 August 2024; Accepted 7 October 2024
Available online 9 October 2024

friendly nature [11]. Among oxides, rare earth orthophosphates ($REPO_4$) has received a lot of attention as an essential inorganic material because of its prospective applications in light-emitting diodes, drug administration, and solar cells [13,14]. Furthermore, since Gd^{3+} possesses half-filled 4f electron shell with a stable structure, $GdPO_4$ is an important host material for doping of lanthanide ions and has great thermal and chemical stability with low phonon energy [7,15]. Due to the paramagnetic behaviour derived from the half-filled 4f electron shell of the Gd^{3+} ion, such materials have also been employed in optical imaging and magnetic resonance [16]. Gd^{3+} ion can be easily replaced by lanthanide ions in the host lattice due to its similar valence and comparable ionic radii. The Tm^{3+} ion has received much attention as a dopant in inorganic host lattice due to its intense blue and near-infrared (NIR) up-conversion emission via numerous energy levels under NIR stimulation. But Tm^{3+} ion singly cannot be excited effectively with 980 nm laser diode excitation. To address this issue, another lanthanide ion, Yb^{3+}, can be employed as a sensitizer due to its larger absorption cross section at 980 nm excitation. Following the excitation of the Yb^{3+} ion, several energy transfer mechanisms from Yb^{3+} to Tm^{3+} takes place, resulting in efficient UC emission at various wavelengths [17]. It is well-established that the optical properties of lanthanide ions depend on its local environment as it allows the parity-forbidden intra-4f electronic transitions of the lanthanide ion to partially allow by mixing the f states with higher electronic configurations. Hence, to realise an effective UC process, it is crucial to use a host lattice with a low phonon energy and low crystal field symmetry [18]. Once the crystal phase of the chosen host lattice is determined, another interesting method to improve UC is to alter the local crystal environment around the lanthanide dopants via the purposeful doping of non-luminescent cationic ions such as Li^+, Mg^{2+} and Zn^{2+} etc. [19–21]. These non-luminescent ions may substitute the cationic ions of the host lattice or occupy the interstitial site around the lanthanide ions, decreasing the local symmetry and boosting UC efficiency. Many studies found that adding Li^+ with Tm^{3+}/Yb^{3+}, Ho^{3+}/Yb^{3+} and Er^{3+}/Yb^{3+} pairs has increased the strength of up-conversion emission as well as optical thermometric properties [19,22–25]. However, higher concentration of Li^+ ions in the host lattice beyond optimal value may lead to increased number of defects in the crystal structure, concentration quenching, cross-relaxation, decreased energy transfer between dopants etc. Such factor contributes significantly in reducing UC emission efficiency of phosphors.

The fluorescence intensity ratio (FIR) based optical thermometry has received a lot of attention in recent decades due to the fact that non-contact high temperature measurement can be performed by measuring the temperature dependency of FIR. This technique compares the UC luminescence intensity emitted from two thermally couple levels (TCLs) or non thermally coupled levels (NTCLs) at various external temperatures [26]. Lanthanide ions are commonly used in FIR techniques due to their ladder like abundant energy levels and luminescence [27]. Temperature sensing properties of luminescent materials doped with RE ions such as Er^{3+}, Tm^{3+}, Nd^{3+}, Ho^{3+}, Pr^{3+}, Dy^{3+}, Tb^{3+}, and Eu^{3+} were extensively studied [28]. For example, in Er^{3+}ion, $^2H_{11/2}$ and $^4S_{3/2}$ levels are used for optical temperature sensing applications as they belong to TCLs. But the smaller energy gap ($\Delta E = \sim 800\ cm^{-1}$) between TCLs of Er^{3+} ion, leads to poor thermal sensitivity as it is directly proportional to energy separation (ΔE) [29]. The experimental findings showed that the FIR technique based on thermally coupled energy levels with a large energy gap ($\sim 2000\ cm^{-1}$) and non-thermally coupled energy levels could be a potential technique for producing high temperature sensitivity [30,31]. Interestingly, $^3F_3$ and $^3H_4$ levels of Tm^{3+} ion has larger energy gap of around 1817 cm^{-1} which is below the maximum limit of 2000 cm^{-1} criteria for TCLs [32]. So these levels of Tm^{3+} ion are expected for higher optical temperature sensing values than $^1G_{4\ (a)}$ and $^1G_{4\ (b)}$ TCLs. It is worth mentioning that, the majority of the energy level pairs created by rare earth ions are non-thermally coupled levels in nature. In fact, the emissions produced from NTCLs are also temperature dependent. NTCL-based technique, as opposed to TCL-based technique, isn't restricted by energy level difference and may thus have higher temperature sensitivity.

In the present work, the UC emission study and optical thermometric performance of $GdPO_4$:Tm^{3+}/Yb^{3+} phosphor with and without Li^+ ions are compared. The mechanisms involved in UC emission are investigated in details using pump photon and energy level diagram. The optical temperature sensing values were calculated using two pairs of NTCLs. Further, anti-counterfeiting and latent figure print detection was also explored.

2. Experimental

2.1. Materials

For the synthesis of phosphors, analytical grade chemicals are utilized without additional purification. Gd_2O_3 (99.9 %), $(NH_4)H_2PO_4$ (99.9 %), Tm_2O_3 (99.9 %), Yb_2O_3 (99.9 %) and Li_2CO_3 (99 %) were purchased from Alfa Aesar.

2.2. Synthesis of Tm^{3+}/Yb^{3+}: $GdPO_4$ and $Tm^{3+}/Yb^{3+}/Li^+$: $GdPO_4$ phosphors

The Tm^{3+}/Yb^{3+} and $Tm^{3+}/Yb^{3+}/Li^+$ codoped $GdPO_4$ phosphors were produced using the solid state reaction approach. All of the raw elements, comprising Gd_2O_3, $(NH_4)H_2PO_4$, Tm_2O_3, Yb_2O3 and Li_2CO_3 were weighed and uniformly mixed and ground for 1 hr in an agate mortar pestle using acetone as the mixing medium. The obtained powder was placed in a clean alumina crucible and heated in an electric furnace for 4 h at an optimized temperature of 1200 °C and cooling down to room temperature. The Tm^{3+} and Yb^{3+} ion concentrations were fixed at 0.3 mol% and 5 mol% respectively, while Li^+ concentrations were varied as 5, 10, and 15 mol% for enhanced luminescence [33,34]. Among all of the synthesized samples, 10 mol% Li^+ concentrations demonstrated the highest UC luminescence and were chosen for further investigation.

2.3. Measurements

X-ray diffraction (XRD) patterns were obtained over a 2θ range of 15°–60° using a Cu K_α (1.5406 Å) radiation source on a high

resolution Rigaku Smartlab X-ray diffractometer. Zeiss Supra 55 Electron Microscope was used to take Field emission scanning electron microscopy (FESEM) images. Using a fast CCD spectrometer (ULS2048 × 64, Avantes, USA) and a 980 nm power tuneable continuous wave (CW) diode laser (max power ~ 2 W), the UC emission spectra were acquired. For the temperature-dependent UC emission experiment, a thermocouple was placed close to the laser point on the sample surface, and the spectra were recorded using a CCD spectrometer. To prevent from heating the material directly, the CW light was chopped by a chopper and the laser beam power was fixed at 63 mW. A built in lab electric furnace was used to raise the sample temperature during the UC measurement. The samples were used in powder form for all measurements.

3. Results and discussion

3.1. Structural and morphological studies

X-ray diffraction analysis was performed to determine the crystal phase and purity of synthesized phosphors. Fig. 1 (a) shows the XRD patterns of 0.3 mol%Tm^{3+}/5 mol%Yb^{3+}/x mol% Li^{+}: $GdPO_4$ (x = 0,5,10,15). The position of all the diffraction peaks were identical with the monoclinic phase of $GdPO_4$ (JCPDS No. 032–0386) with space group P21/n (14). Additionally, two impurity peaks were also detected in Li^{+} codoped samples at 32.58 and 34.82°, which shows identical match with hexagonal crystal phase of lithium oxide as shown in Fig. 1(b). These peaks were observed due to higher concentrations of Li^{+} ions in the sample. From Fig. 1 (a), it can be seen that the peak corresponding to (111) plane viz. 25.80° increases with increasing Li^{+} ion concentrations. The change in peak intensity indicates change in the preferred orientation of the crystals [35]. Such orientation occurs due to alignment of crystallites in certain direction, which leads to some lattice planes more favourable to diffract the X-rays. That increases the intensity for peak corresponding to those planes. After codoping with Li^{+} ions, the crystallites tend to align with their (111) planes, which resulted increased intensity for peak at 25.80°.

The surface morphology of the synthesized phosphors have been studied using field emission scanning electron microscopy. The typical FESEM images of 0.3 mol%Tm^{3+}/5 mol%Yb^{3+}: $GdPO_4$ and 0.3 mol%Tm^{3+}/5 mol%Yb^{3+}/10 mol% Li^{+}:$GdPO_4$ phosphors are shown in Fig. 2 (a) and (b) respectively. The surface of Li^{+} undoped phosphor shows irregular and agglomerated particles while codoping of Li^{+} ion resulted non-uniform and larger particles. At increasing particle size, the surface-to-volume ratio also decreases, which is also expected to contribute in enhancement of UC emissions. Several research groups have reported increased particle size upon codoping of Mg^{2+} and Li^{+} ions [25,36–38].

3.2. Upconversion luminescence study and mechanism

The UC emission spectra acquired by altering Li^{+} concentrations in Tm^{3+}/Yb^{3+}:$GdPO_4$ phosphor using a 980 nm laser diode with a pump power of 63 mW are shown in Fig. 3(a). The spectra comprises a dominant blue emission band at 478 nm caused by the $^1G_4 \rightarrow {}^3H_6$ transition, and some weak red emission bands at 648 and 692 nm resulted from $^1G_4 \rightarrow {}^3F_4$ and $^3F_3 \rightarrow {}^3H_6$ transitions of the Tm^{3+} ion, respectively [37,39]. The intensity of the emission bands increases with increasing Li^{+} ion concentrations up to 10 mol%, after that it starts declining due to the concentration quenching effect [40,41]. The Li^{+} ions can either replace the cationic ion in the host lattice or occupy the interstitial sites around the lanthanide ions, decreasing the local symmetry and increasing UC efficiency [18]. The maximum UC emission is observed for 10 mol% Li^{+} ion concentrations along with 0.3 mol%Tm^{3+} and 5 mol%Yb^{3+} ions.

The energy levels diagram could be used to describe the key UC processes. Since Yb^{3+} ion has larger absorption cross-section for 980 nm excitation, so it is used as a sensitizer for energy transfer to Tm^{3+} ions. As shown in Fig. 3(b), after absorbing photons from 980 nm excitation, Yb^{3+} ion raised to its excited $^2F_{5/2}$ level. Two consecutive energy transfer process ET (1) and ET (2) from Yb^{3+} to Tm^{3+}

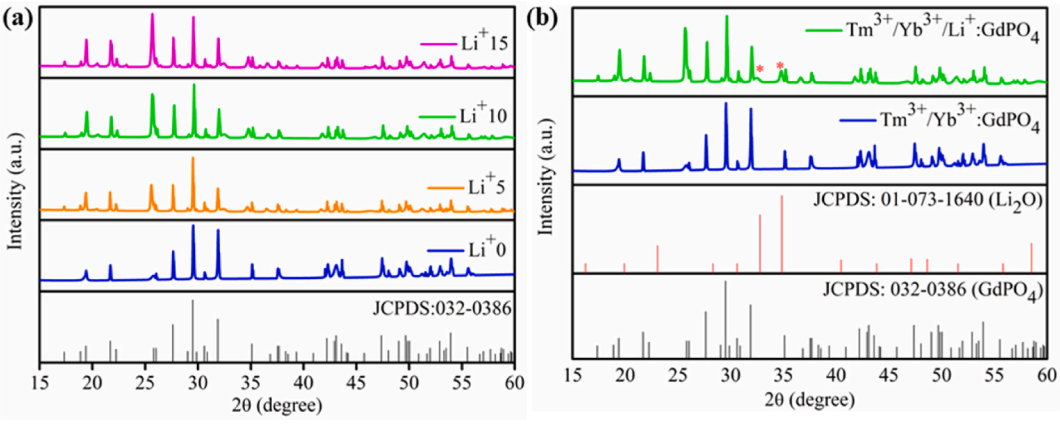

Fig. 1. (a) XRD patterns of 0.3 mol%Tm^{3+}/5 mol%Yb^{3+}/x mol% Li^{+}: $GdPO_4$ (x = 0,5,10,15) samples, (b) XRD pattern of Li^{+} undoped and codoped samples compared with standard JCPDS file of $GdPO_4$ and Li_2O, the impurity peaks are indicated with asterisk.

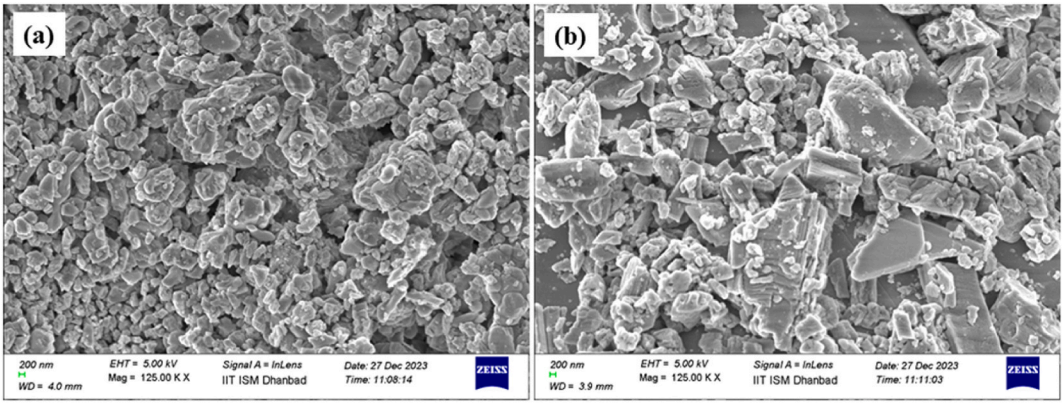

Fig. 2. FESEM images of (a) Tm^{3+}/Yb^{3+}: $GdPO_4$; (b) $Tm^{3+}/Yb^{3+}/Li^{+}$: $GdPO_4$ phosphors.

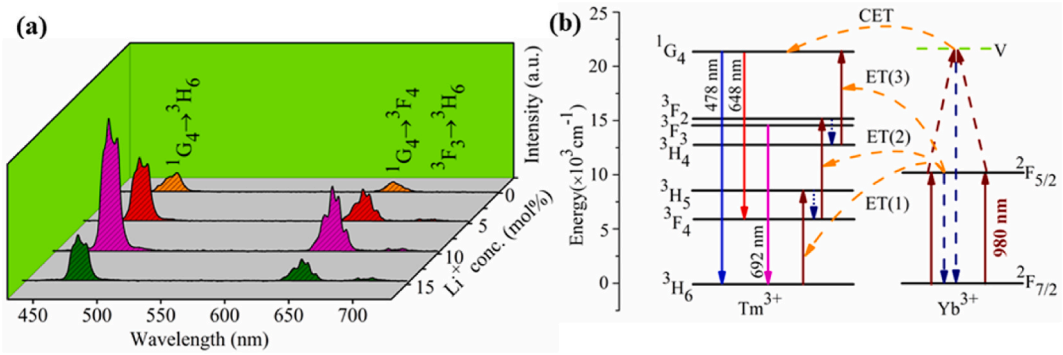

Fig. 3. (a) Upconversion emission spectra of $GdPO_4$:0.3 mol%Tm^{3+}/5mol% Yb^{3+}/x mol% Li^{+} (x = 0, 5, 10 and 15) phosphors; (b) Possible UC mechanism for observed emissions bands in Tm^{3+}/Yb^{3+}:$GdPO_4$ system.

ions leads the Tm^{3+} population to $^3F_2$ excited level from their ground $^3H_6$ level [40]. The population of $^3F_2$ level relaxes non radiatively to $^3H_4$ level via intermediate $^3F_3$ level. A radiative transition $^3F_3 \rightarrow {}^3H_6$ leads the emission of a photon at 692 nm. The $^3F_3$ level is thermally coupled with the lower $^3H_4$ level, which benefits the population of $^3F_3$ level upon thermal excitation as TCLs follows Boltzman's population distribution. The third excited state absorption ET (3) populates the Tm^{3+} ions to $^1G_4$ level from lower $^3H_4$ level. This populated level relaxes via radiative transition to $^3H_6$ and $^3F_4$ levels by emitting photons of 478 nm (blue) and 648 nm (red) respectively. As from energy level diagram, the emissions at 478 and 648 nm are originating from absorption of three NIR photons while emission at 692 nm is due to two photons absorption process [42].

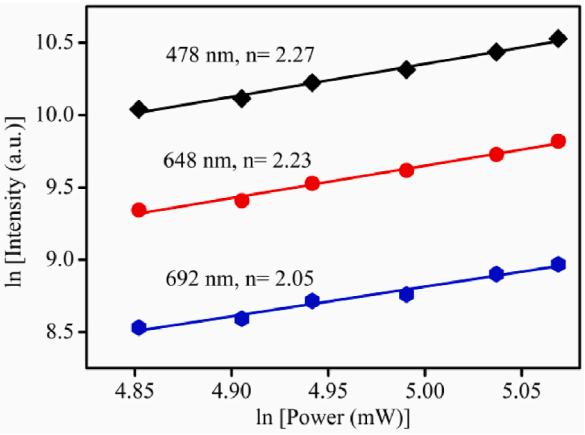

Fig. 4. ln-ln plot of UC emission intensity versus pump power for 0.3 mol%Tm^{3+}/5 mol% Yb^{3+}:$GdPO_4$ phosphor.

It is well known that, the relation between the UC emission intensity (I) and excitation power (P) can be used to determine the number of NIR photons participating in the population of the emitting levels for an unsaturated UC process. It can be written as [43];

$$I \propto P^{n} \tag{1}$$

where, n is the number of pump photons engaged in the UC luminescence process. Fig. 4 shows the ln-ln plot of emission intensity versus pump power for all three transitions. Upon linear fitting, the slope values are found to be 2.27, 2.23 and 2.05 for 478, 648 and 692 nm emissions respectively.

The pump power analysis as shown in Fig. 4 confirms that all the emissions are from 2-photon absorption process but energy level diagram (Fig. 3(b)) indicates that the emission at 478, 648 nm are from 3-photon absorption process, while emission at 692 nm is due to 2-photon process. The reduced value of pump photons for 478 and 648 nm emissions is due to involvement of cooperative energy transfer (CET) channels in the system. Energy level diagram shows two different possible excitation mechanisms for $^{1}G_4$ level of Tm^{3+}ion viz. cooperative energy transfer and simple energy transfer processes (ET-3). If we consider energy levels matching then energy transfer process ET-3 can also be possible. But from experimental data, calculated slope values are found to be nearly '2' which indicates that CET process is dominated over ET-3 process for the emissions at 478 and 648 nm. While, emissions at 692 nm is due to ET-2 process which requires only two NIR excitation photons. This is consistent with findings from other Tm^{3+}/Yb^{3+} codoped materials [37,44]. The CET process involves the simultaneous transfer of excitation energy from two excited neighbouring Yb^{3+}ions to populate the $^{1}G_4$ excited level of Tm^{3+} ion without going through the real intermediate states [42].

3.3. Lifetime studies

The lifetime of $^{1}G_4$ level of Tm^{3+} ion in 0.3 mol% Tm^{3+}/5 mol% Yb^{3+}: $GdPO_4$ and 0.3 mol% Tm^{3+}/5 mol% Yb^{3+}/10 mol% Li^{+}: $GdPO_4$ phosphor for the emission at 478 nm under 980 nm laser diode excitation is shown in Fig. 5 (a) and (b) respectively. The measured decay curves can be well fitted to the following exponential equation [45];

$$I = I_0 \ \exp\left(-\frac{t}{\tau}\right) \tag{2}$$

where, I and I_0 are the decay intensities at time t and time zero respectively and τ is the lifetime of emitting level. The lifetime of $^{1}G_4$ level in without Li^{+} sample is found to be 114 μS, while it reduces to 92 μS with Li^{+} ions. The codoping of Li^{+} ions tailors the local crystal field around the Tm^{3+} ions. Modification in crystal field increases the radiative transition probability from excited level to ground level. Increased transition probability reduces the lifetime of the emitting level.

3.4. Optical thermometry

The temperature-dependent upconversion spectra of Tm^{3+}/Yb^{3+}:$GdPO_4$ phosphor was investigated in the temperature range of 301–713 K. The spectra were obtained by exciting the sample with a 980 nm diode laser at fixed power of 63 mW. The results are presented in Fig. 6(a). To reduce the heat induced by the 980 nm laser, a lower excitation power is employed. As shown in Fig. 6(a), the emission intensity of 478 and 648 nm decreases at increasing temperature, while the intensity of 692 nm emission band shows opposite behaviour. The decrease in intensity is due to the increase in non radiative relaxation at elevated temperature whereas; the increment in intensity of 692 nm is due to thermal excitation. Thermal excitation causes the population of $^{3}F_3$ level from $^{3}H_4$, as both are thermally coupled levels. Such levels are subjected to the Boltzmann's population distribution law. Although, TCLs are commonly used in FIR technology, the temperature measurement method based on TCLs has significant disadvantages. As, these levels are restricted by energy separation of 200–2000 cm^{-1}. Generally, higher ΔE leads greater sensitivity, so it is challenging to obtain higher sensitivity while considering smaller energy gap between TCLs.

Most of the energy levels found in lanthanide ions are inherently non-thermally coupled, and the emission from these levels is

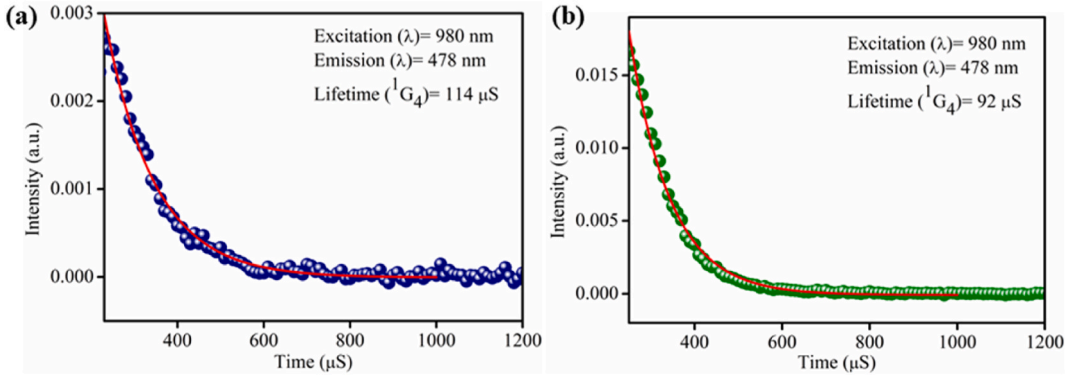

Fig. 5. Lifetime of $^{1}G_4$ level of Tm^{3+} ion under 980 nm laser diode excitation in (a) Tm^{3+}/Yb^{3+}:$GdPO_4$; (b) $Tm^{3+}/Yb^{3+}/Li^{+}$:$GdPO_4$ phosphors.

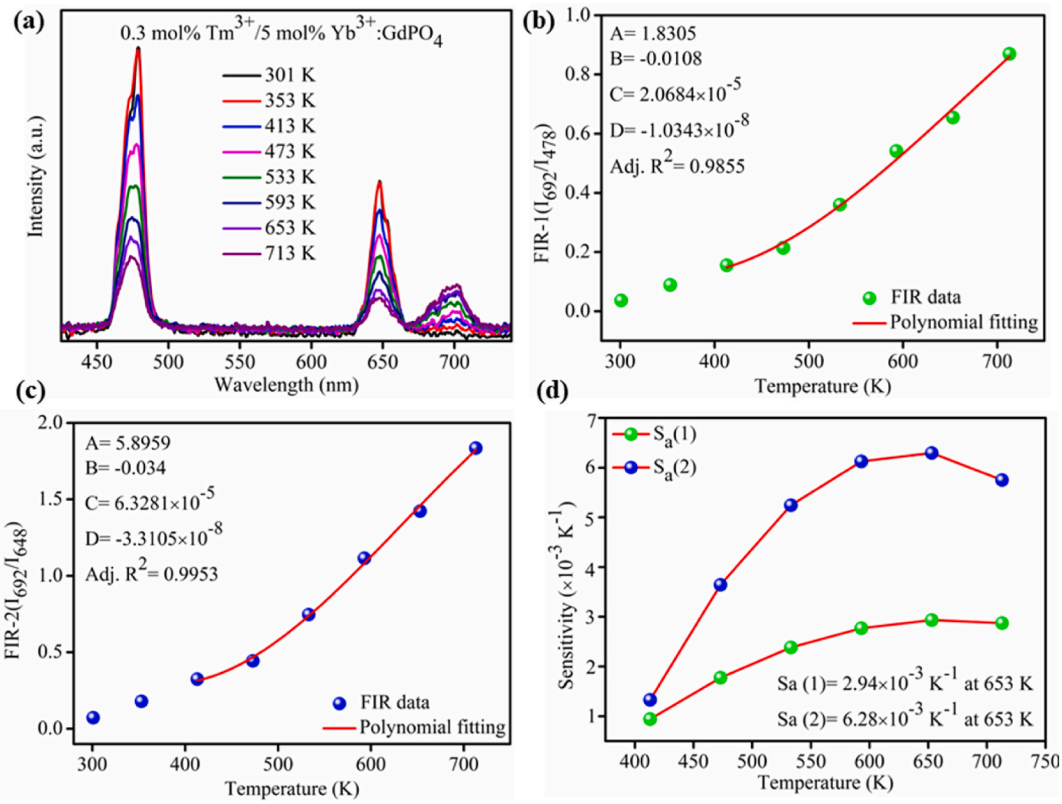

Fig. 6. (a) Temperature dependent UC spectra of 0.3 mol%Tm^{3+}/5 mol% Yb^{3+}:$GdPO_4$ sample in the range 301–713 K; (b, c) Polynomial fitting of FIR (1) and FIR (2) data versus temperature; (d) Absolute sensitivities as a function of temperature.

strongly dependent on temperature. Hence, the emission from $^3F_3$ (692 nm) and $^1G_4$ (478, 648 nm) levels are considered for FIR based optical thermometric studies. The FIR of 692nm/478 nm and 692nm/648 nm emissions is indicated as FIR (1) and FIR (2) respectively.

Since, the thermal excitation cannot populate the NTCLs due to larger energy gap, so temperature dependent FIR can be fitted with following polynomial function [39,46];

$$FIR = A + BT + CT^2 + DT^3 \tag{3}$$

Where A, B, C, D are constants whose values are determined by fitting the experimental temperature dependent FIR data with Eq. (3). The polynomial fitting of FIR (1) and FIR (2) data with temperature is shown in Fig. 6(b) and (c) respectively. Since, FIR is almost constant with temperature from 301 to 413 K, it means that the material is not sensitive to temperature changes in this range, making it difficult to use for practical temperature sensing applications. Therefore FIR data were fitted from 413 to 713 K temperature.

The fitting gives the FIR (1) = (1.8305)–(0.0108) T+ (2.0684 × 10^{-5}) T^2- (1.0343 × 10^{-8}) T^3 and FIR (2) = (5.8959)–(0.034) T+ (6.3281 × 10^{-5}) T^2- (3.3105 × 10^{-8}) T^3 with adj. R^2 = 0.9855 and 0.9953 respectively.

The sensitivity is an important parameter which is defined as;

$$S_a = \frac{d(FIR)}{dT} = B + 2CT + 3DT^2 \tag{4}$$

The plot of both the sensitivities S_a (1) and S_a (2) corresponding to FIR (1) and FIR (2) as a function of temperature is shown in Fig. 6 (d). The maximum absolute sensitivity of 2.94 × 10^{-3} K^{-1} and 6.28 × 10^{-3} K^{-1} at 653 K are observed corresponding to FIR (1) and FIR (2) respectively.

In order to compare the observed sensitivity with 0.3 mol%Tm^{3+}/5 mol%Yb^{3+}/10 mol% Li^+:$GdPO_4$ phosphor, similar analysis has been performed and shown in Fig. 7(a–d). The sensitivity graph shown in Fig. 7 (d) represents the S_a (1) and S_a (2) corresponding to FIR (1) and FIR (2) data. The maximum absolute sensitivity of 10.38 × 10^{-3} K^{-1} and 18.71 × 10^{-3} K^{-1} at 713 K are observed corresponding to FIR (1) and FIR (2).

The relative sensitivity of the synthesized phosphors has also been calculated and found that Li^+ undoped sample shows a maximum relative sensitivity of 8.29 × 10^{-3} K^{-1} while Li^+ codoped sample shows a maximum relative sensitivity of 11.76 × 10^{-3} K^{-1} at 473 K temperature. The relative sensitivity graph is shown in supplementary data of this manuscript as Fig. S1.

The above discussion shows that, codoping of 10 mol% Li^+ ions in Tm^{3+}/Yb^{3+}:$GdPO_4$ phosphor not only increases the UC emission but also increased its temperature sensing ability. Table 1 compares the obtained sensing results with previously reported Tm^{3+} based

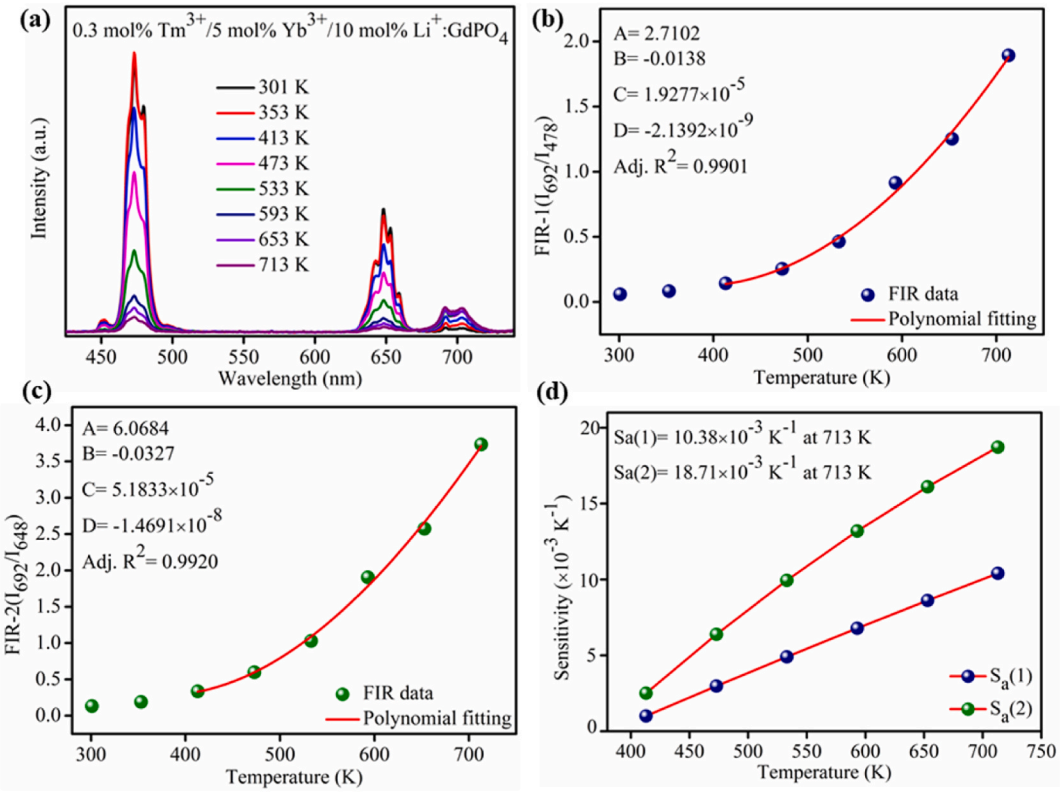

Fig. 7. (a) Temperature dependent UC spectra of 0.3 mol%Tm^{3+}/5 mol%Yb^{3+}/10 mol% Li^{+}:$GdPO_4$ phosphor in temperature range 301–713 K; (b, c) Polynomial fitting of FIR (1) and FIR (2) data versus temperature; (d) Absolute sensitivities as a function of temperature.

materials to insight its suitability in non-contact optical thermometers.

3.5. CIE colour coordinates study

The temperature dependent UC data also provide the information about change in CIE chromaticity coordinates upon varying temperature. Fig. 8 (a, b) shows the CIE diagrams of Tm^{3+}/Yb^{3+} and $Tm^{3+}/Yb^{3+}/Li^{+}$ codoped $GdPO_4$ phosphors in the temperature range 301–773 K respectively. In Li^{+} undoped sample, there is very minor change in coordinates i.e. from (0.31, 0.30) to (0.32, 0.32), while in Li^{+} codoped sample coordinates shifted from blue (0.25, 0.21) to white (0.32, 0.32). Due to of its colour tuning nature this can be used as warning sign indicator at high-temperature environments.

3.6. Latent fingerprint visualization and security ink applications

The synthesized 0.3 mol% Tm^{3+}/5 mol% Yb^{3+}: $GdPO_4$ and 0.3 mol% Tm^{3+}/5 mol% Yb^{3+}/10 mol% Li^{+}: $GdPO_4$ phosphors were tested for visualization of latent fingerprints on glass surface. The step by step process of development and detection of latent fingerprints can be found in our previous work [45].

Fig. 9 (a) and (b) are the latent images in daylight, while Fig. 9 (a') and (b') shows the powder dusted images with Li^{+} undoped and codoped phosphors and illuminated with 980 nm laser diode respectively. Notably, both phosphors exhibit the fingerprints in blue colour, but Li^{+} codoped phosphor shows more contrast image (Fig. 9(b')) than Li^{+} free sample (Fig. 9(a')). This results show the suitability of prepared phosphors in security applications.

Furthermore, the synthesized phosphors have been tested in anti-counterfeiting applications as fluorescent ink. The security ink was prepared using the method given by Park et al. [51]. Fig. 9 (c) and (d) demonstrates the world "IIT" written on plain white paper using Li^{+} free and codoped samples, which is invisible in daylight. While illuminating this paper with 980 nm laser diode resulted text in high contrast blue colour as shown in Fig. 9 (c') and (d') respectively. Hence, the prepared phosphor can also be used to create security markers to prevent from counterfeiting of food, goods and currency.

4. Conclusions

The monoclinic phase of Tm^{3+}/Yb^{3+}:$GdPO_4$ phosphor codoped with various concentrations of Li^{+} ion was successfully synthesized

Table 1
FIR based absolute temperature sensitivities obtained in reported literatures.

UC phosphors	Absolute sensitivity (S_a) ($\times 10^{-3}K^{-1}$) (K)	Temperature range(K)	References
$GdPO_4$:Tm^{3+}/Yb^{3+}/Li^{+}	18.71 (713)	413–713	**This work**
$GdPO_4$:Tm^{3+}/Yb^{3+}	6.28 (653)	413–713	**This work**
$Ca_9Y(PO_4)_7$:Tm^{3+}/Yb^{3+}	11.30 (823)	323–823	[47]
$SrWO_4$:Tm^{3+}/Yb^{3+}	6.17 (323)	308–573	[48]
LuAG:Tm^{3+}/Yb^{3+}	5.55 (1023)	298–1023	[33]
Y_2O_3:Tm^{3+}/Yb^{3+}	2.80 (298)	303–573	[44]
Y_2SiO_5:Tm^{3+}/Yb^{3+}	1.25 (473)	298–473	[49]
YF_3:Tm^{3+}/Yb^{3+}	1.01 (750)	300–750	[50]

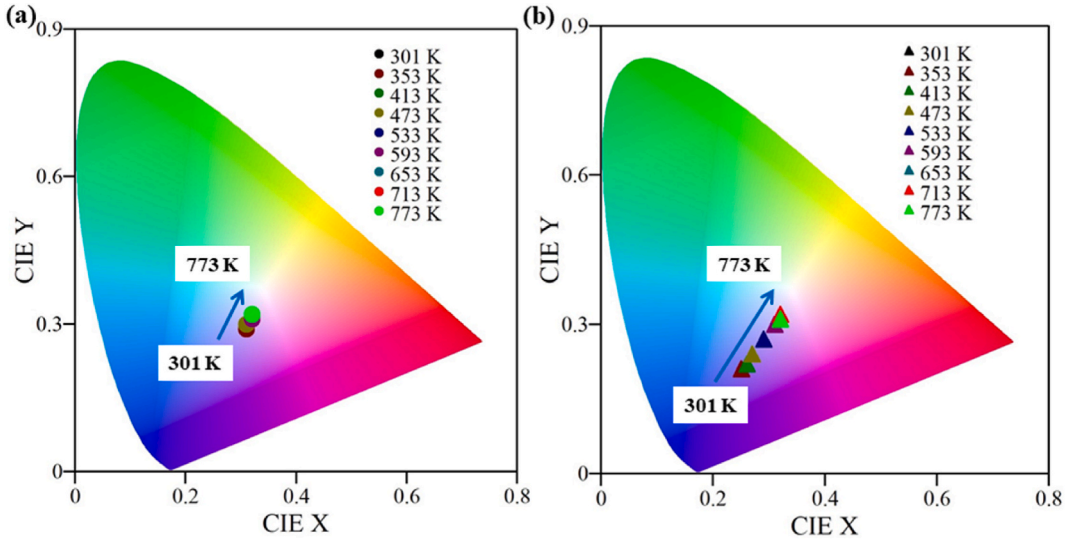

Fig. 8. Temperature dependent CIE colour coordinate diagrams of (a) 0.3 mol% Tm^{3+}/5 mol% Yb^{3+}: $GdPO_4$; (b) 0.3 mol% Tm^{3+}/5 mol% Yb^{3+}/10 mol% Li^{+}: $GdPO_4$ phosphors. (For interpretation of the references to colour in this figure legend, the reader is referred to the Web version of this article.)

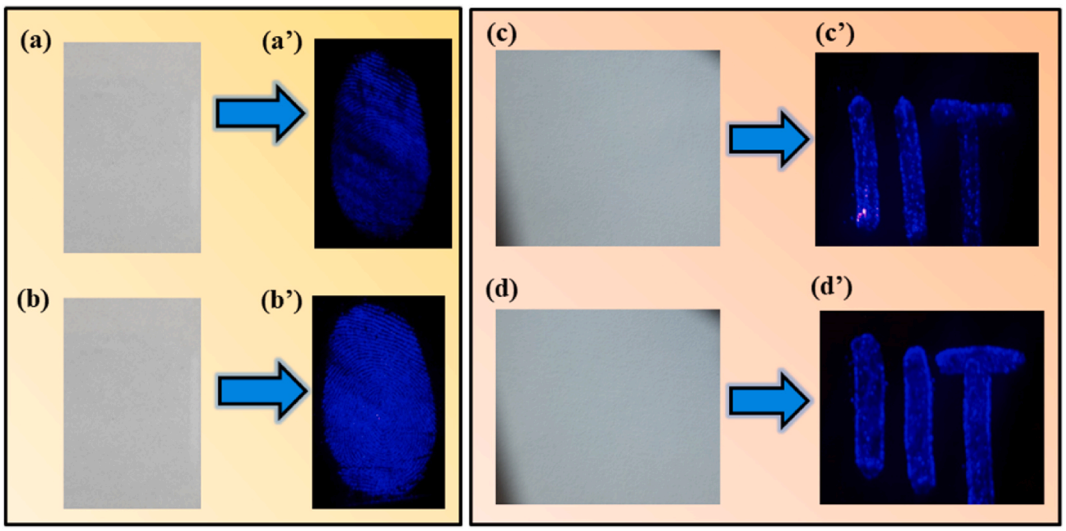

Fig. 9. (a, b) Latent fingerprints under daylight; (a', b') Powder dusted images upon 980 nm laser excitation; (c, d) Daylight photograph of written white plain papers with security ink made of without and with Li^{+} codoped samples; (c', d') same photographs under 980 nm laser diode illumination.

using solid state reaction method. The UC spectra through 980 nm excitation shows a strong blue emission band at 478 nm originating from $^1G_4 \rightarrow {}^3H_6$ transition and some weaker red bands at 648 and 692 nm due to $^1G_4 \rightarrow {}^3F_4$ and $^3F_3 \rightarrow {}^3H_6$ transition of Tm^{3+} ion respectively. Temperature dependent UC spectra were measured to investigate temperature sensing performance of the synthesized phosphors. The temperature sensing was studied through two FIR cases of 692nm/478 nm termed as FIR (1), and 692nm/648 nm termed as FIR (2). Li^+ undoped phosphor shows a maximum absolute sensitivity of $2.94 \times 10^{-3}\ K^{-1}$ and $6.28 \times 10^{-3}\ K^{-1}$ at 653 K temperature for FIR (1) and FIR (2) respectively. Whereas, 10 mol% Li^+ codoped phosphor, shows a maximum absolute sensitivity of $10.38 \times 10^{-3}\ K^{-1}$ and $18.71 \times 10^{-3}\ K^{-1}$ at 713 K for FIR (1) and FIR (2) cases respectively. It can be concluded that, Li^+ codoping improved not only the efficiency of UC emission but also their optical thermometry properties. Additionally, the possible application of prepared phosphors in latent fingerprint detection and anti-counterfeiting shows satisfactory results.

CRediT authorship contribution statement

Madan M. Upadhyay: Writing – original draft, Visualization, Validation, Software, Methodology, Investigation, Formal analysis, Data curation, Conceptualization. **Kaushal Kumar:** Writing – review & editing, Visualization, Validation, Supervision, Resources, Project administration, Funding acquisition.

Declaration of competing interest

The authors declare that they have no known competing financial interests or personal relationships that could have appeared to influence the work reported in this paper.

Acknowledgements

Madan M. Upadhyay is grateful to Indian Institute of Technology (ISM) Dhanbad for providing financial support in form of Senior Research Fellowship (SRF). Authors also acknowledge to DST-SERB, New Delhi India for providing experimental facilities. K. Kumar acknowledges to DST project No.: CRG/2023/006161 for financial support.

Appendix A. Supplementary data

Supplementary data to this article can be found online at https://doi.org/10.1016/j.heliyon.2024.e39081.

References

[1] A. Ghazy, M. Safdar, M. Lastusaari, H. Savin, M. Karppinen, Advances in upconversion enhanced solar cell performance, Sol. Energy Mater. Sol. Cells 230 (2021) 111234, https://doi.org/10.1016/j.solmat.2021.111234.
[2] J. Zhang, B. Ji, G. Chen, Z. Hua, Upconversion luminescence and discussion of sensitivity improvement for optical temperature sensing application, Inorg. Chem. 57 (2018) 5038–5047, https://doi.org/10.1021/acs.inorgchem.8b00102.
[3] M. You, J. Zhong, Y. Hong, Z. Duan, M. Lin, F. Xu, Inkjet printing of upconversion nanoparticles for anti-counterfeit applications, Nanoscale 7 (2015) 4423–4431, https://doi.org/10.1039/C4NR06944G.
[4] B. Zhou, B. Shi, D. Jin, X. Liu, Controlling upconversion nanocrystals for emerging applications, Nat. Nanotechnol. 10 (2015) 924–936, https://doi.org/10.1038/nnano.2015.251.
[5] F. Wang, D. Banerjee, Y. Liu, X. Chen, X. Liu, Upconversion nanoparticles in biological labeling, imaging, and therapy, Analyst 135 (2010) 1839, https://doi.org/10.1039/c0an00144a.
[6] F. Wang, X. Liu, Recent advances in the chemistry of lanthanide-doped upconversion nanocrystals, Chem. Soc. Rev. 38 (2009) 976, https://doi.org/10.1039/b809132n.
[7] T. Grzyb, A. Gruszeczka, S. Lis, Up-conversion luminescence of Yb3+ and Er3+ doped YPO4, LaPO4 and GdPO4 nanocrystals, J. Lumin. 175 (2016) 21–27, https://doi.org/10.1016/j.jlumin.2016.02.021.
[8] X. Wang, X. Li, H. Zhong, S. Xu, L. Cheng, J. Sun, J. Zhang, L. Li, B. Chen, Up-conversion luminescence, temperature sensing properties and laser-induced heating effect of Er3+/Yb3+ co-doped YNbO4 phosphors under 1550 nm excitation, Sci. Rep. 8 (2018) 5736, https://doi.org/10.1038/s41598-018-23981-4.
[9] Y. Tian, Y. Tian, P. Huang, L. Wang, Q. Shi, C. Cui, Effect of Yb3+ concentration on upconversion luminescence and temperature sensing behavior in Yb3+/Er3+ co-doped YNbO4 nanoparticles prepared via molten salt route, Chem. Eng. J. 297 (2016) 26–34, https://doi.org/10.1016/j.cej.2016.03.149.
[10] F. Wang, X. Liu, Recent advances in the chemistry of lanthanide-doped upconversion nanocrystals, Chem. Soc. Rev. 38 (2009) 976–989, https://doi.org/10.1039/b809132n.
[11] L. Guo, X. Zheng, S. Zhang, B. Zhao, Y. Wang, Upconversion- and cathodo-luminescence properties of Yb3+/Ho3+/Li+ tridoped Lu6O5F8 nanoparticles, Mater. Res. Bull. 86 (2017) 1–4, https://doi.org/10.1016/j.materresbull.2016.09.011.
[12] S. Liu, J. Cui, L. Liu, W. You, M.C. Parmar, Q. Zeng, R. Wang, X. Ye, High-purity upconversion output color and excellent optical thermometry performance of lanthanide-doped Ba3Y4O9, J. Lumin. 213 (2019) 174–183, https://doi.org/10.1016/j.jlumin.2019.04.056.
[13] Y. Wang, H. Zhang, S. Qu, C. Su, Downconversion and upconversion emissions of GdPO4:Yb3+/Tb3+ and its potential applications in solar cells, J. Alloys Compd. 677 (2016) 266–270, https://doi.org/10.1016/j.jallcom.2016.03.242.
[14] M.A. Hassairi, A. Garrido Hernández, M. Dammak, D. Zambon, G. Chadeyron, R. Mahiou, Tuning white upconversion emission in GdPO4:Er/Yb/Tm phosphors, J. Lumin. 203 (2018) 707–713, https://doi.org/10.1016/j.jlumin.2018.07.024.
[15] V. Kumar, P. Rani, D. Singh, S. Chawla, Efficient multiphoton upconversion and synthesis route dependent emission tunability in GdPO 4 :Ho 3+ , Yb 3+ nanocrystals, RSC Adv. 4 (2014) 36101–36105, https://doi.org/10.1039/C4RA04795H.
[16] I. Suryawanshi Pushpendra, S. Srinidhi, S. Singh, R. Kalia, R.K. Kunchala, S.L. Mudavath, B.S. Naidu, Downshifting and upconversion dual mode emission from lanthanide doped GdPO4 nanorods for unclonable anti-counterfeiting, Mater. Today Commun. 26 (2021) 102144, https://doi.org/10.1016/j.mtcomm.2021.102144.

[17] F. Pandozzi, F. Vetrone, J.-C. Boyer, R. Naccache, J.A. Capobianco, A. Speghini, M. Bettinelli, A spectroscopic analysis of blue and ultraviolet upconverted emissions from Gd 3 Ga 5 O 12 :Tm 3+ , Yb 3+ nanocrystals, J. Phys. Chem. B 109 (2005) 17400–17405, https://doi.org/10.1021/jp052192w.
[18] G. Chen, H. Qiu, P.N. Prasad, X. Chen, Upconversion nanoparticles: design, nanochemistry, and applications in theranostics, Chem. Rev. 114 (2014) 5161–5214, https://doi.org/10.1021/cr400425h.
[19] T. Peng, Y. Cao, H. Cui, Y. Zhang, Y. Wang, X. Li, X. Zhang, B. Chen, Enhancement of green upconversion luminescence and temperature sensitivity of Zr2(WO4)(PO4)2:Er3+,Yb3+ phosphors by co-doping Li+ ions, J. Alloys Compd. 893 (2022) 162345, https://doi.org/10.1016/j.jallcom.2021.162345.
[20] S. Sinha, M.K. Mahata, K. Kumar, Enhancing the upconversion luminescence properties of Er 3+ –Yb 3+ doped yttrium molybdate through Mg 2+ incorporation: effect of laser excitation power on temperature sensing and heat generation, New J. Chem. 43 (2019) 5960–5971, https://doi.org/10.1039/C9NJ00760A.
[21] A.K. Choudhary, A. Dwivedi, A. Bahadur, S.B. Rai, Enhanced upconversion from Er3+/Yb3+ co-doped alkaline earth aluminates phosphor in presence Zn2+: a comparative study, J. Lumin. 210 (2019) 135–141, https://doi.org/10.1016/j.jlumin.2019.02.035.
[22] Q. Qiang, S. Du, X. Ma, W. Chen, G. Zhang, Y. Wang, A temperature sensor based on the enhanced upconversion luminescence of Li + doped NaLuF 4 :Yb 3+ , Tm 3+/Er 3+ nano/microcrystals, Dalt. Trans. 47 (2018) 8656–8662, https://doi.org/10.1039/C8DT00928G.
[23] B.P. Singh, A.K. Parchur, R.S. Ningthoujam, P.V. Ramakrishna, S. Singh, P. Singh, S.B. Rai, R. Maalej, Enhanced up-conversion and temperature-sensing behaviour of Er 3+ and Yb 3+ co-doped Y 2 Ti 2 O 7 by incorporation of Li + ions, Phys. Chem. Chem. Phys. 16 (2014) 22665–22676, https://doi.org/10.1039/C4CP02949F.
[24] M.L. Debasu, J.C. Riedl, J. Rocha, L.D. Carlos, The role of Li + in the upconversion emission enhancement of (YYbEr) 2 O 3 nanoparticles, Nanoscale 10 (2018) 15799–15808, https://doi.org/10.1039/C8NR03608J.
[25] M.Y.A. Yagoub, H.C. Swart, E. Coetsee, The role of Li+ interstitial ions in up-conversion intensity of CaF2:Yb3+, Tb3+ phosphors, Mater. Res. Bull. 156 (2022) 111986, https://doi.org/10.1016/j.materresbull.2022.111986.
[26] X. Wang, Q. Liu, Y. Bu, C.-S. Liu, T. Liu, X. Yan, Optical temperature sensing of rare-earth ion doped phosphors, RSC Adv. 5 (2015) 86219–86236, https://doi.org/10.1039/C5RA16986K.
[27] J. Zhong, D. Chen, Y. Peng, Y. Lu, X. Chen, X. Li, Z. Ji, A review on nanostructured glass ceramics for promising application in optical thermometry, J. Alloys Compd. 763 (2018) 34–48, https://doi.org/10.1016/j.jallcom.2018.05.348.
[28] Y. Zhao, X. Wang, Y. Zhang, Y. Li, X. Yao, Optical temperature sensing of up-conversion luminescent materials: fundamentals and progress, J. Alloys Compd. 817 (2020) 152691, https://doi.org/10.1016/j.jallcom.2019.152691.
[29] H. Lv, P. Du, W. Li, L. Luo, Tailoring of upconversion emission in Tm 3+/Yb 3+ -codoped Y 2 Mo 3 O 12 submicron particles via thermal stimulation engineering for non-invasive thermometry, ACS Sustain. Chem. Eng. 10 (2022) 2450–2460, https://doi.org/10.1021/acssuschemeng.1c07323.
[30] S. Liu, H. Ming, J. Cui, S. Liu, W. You, X. Ye, Y. Yang, H. Nie, R. Wang, Color-Tunable upconversion luminescence and multiple temperature sensing and optical heating properties of Ba 3 Y 4 O 9 :Er 3+/Yb 3+ phosphors, J. Phys. Chem. C 122 (2018) 16289–16303, https://doi.org/10.1021/acs.jpcc.8b04180.
[31] J. Tang, P. Du, W. Li, L. Luo, Boosted thermometric performance in NaGdF4:Er3+/Yb3+ upconverting nanorods by Fe3+ ions doping for contactless nanothermometer based on thermally and non-thermally coupled levels, J. Lumin. 224 (2020) 117296, https://doi.org/10.1016/j.jlumin.2020.117296.
[32] S. Chen, W. Song, J. Cao, F. Hu, H. Guo, Highly sensitive optical thermometer based on FIR technique of transparent NaY2F7:Tm3+/Yb3+ glass ceramic, J. Alloys Compd. 825 (2020) 154011, https://doi.org/10.1016/j.jallcom.2020.154011.
[33] H. Zhou, N. An, K. Zhu, J. Qiu, L. Yue, L.-G. Wang, L. Ye, Optical temperature sensing properties of Tm3+/Yb3+ co-doped LuAG polycrystalline phosphor based on up-conversion luminescence, J. Lumin. 229 (2021) 117656, https://doi.org/10.1016/j.jlumin.2020.117656.
[34] G. Chen, R. Lei, F. Huang, H. Wang, S. Zhao, S. Xu, Effects of Tm 3+ concentration on upconversion luminescence and temperature-sensing behavior in Tm 3+/Yb 3+ :Y 2 O 3 nanocrystals, Luminescence 33 (2018) 1262–1267, https://doi.org/10.1002/bio.3544.
[35] H. Chen, D. Li, L. Zhang, G. Bai, S. Xu, L. Chen, Remarkable enhancement of upconversion emissions by thermal stimulation in Er-doped Yb 2 Mo 3 O 12 microcrystals, J. Appl. Phys. 129 (2021) 143101, https://doi.org/10.1063/5.0046818.
[36] R. Dey, A. Kumari, A.K. Soni, V.K. Rai, CaMoO4:Ho3+–Yb3+–Mg2+ upconverting phosphor for application in lighting devices and optical temperature sensing, Sensors Actuators B Chem 210 (2015) 581–588, https://doi.org/10.1016/j.snb.2015.01.007.
[37] R.S. Yadav, S.J. Dhoble, S.B. Rai, Enhanced photoluminescence in Tm3+, Yb3+, Mg2+ tri-doped ZnWO4 phosphor: three photon upconversion, laser induced optical heating and temperature sensing, Sensors Actuators, B Chem. 273 (2018) 1425–1434, https://doi.org/10.1016/j.snb.2018.07.049.
[38] G. Chen, R. Lei, S. Xu, H. Wang, S. Zhao, F. Huang, Y. Tian, Effect of Li + ion concentration on upconversion emission and temperature sensing behavior of La 2 O 3 :Er 3+ phosphors, J. Rare Earths 36 (2018) 119–124, https://doi.org/10.1016/j.jre.2017.03.004.
[39] W. Gao, W. Ge, J. Shi, X. Chen, Y. Li, A novel upconversion optical thermometers derived from non-thermal coupling levels of CaZnOS:Tm/Yb phosphors, J. Solid State Chem. 297 (2021) 122063, https://doi.org/10.1016/j.jssc.2021.122063.
[40] X. Tu, J. Xu, M. Li, T. Xie, R. Lei, H. Wang, S. Xu, Color-tunable upconversion luminescence and temperature sensing behavior of Tm3+/Yb3+ codoped Y2Ti2O7 phosphors, Mater. Res. Bull. 112 (2019) 77–83, https://doi.org/10.1016/j.materresbull.2018.12.008.
[41] A. Zhou, F. Song, F. Song, M. Feng, K. Adnan, D. Ju, X. Wang, Optical thermometry using fluorescence intensities multi-ratios in NaGdTiO4:Yb3+/Tm3+ phosphors, Opt. Mater. 78 (2018) 438–444, https://doi.org/10.1016/j.optmat.2018.02.047.
[42] D. Li, Y. Wang, X. Zhang, K. Yang, L. Liu, Y. Song, Optical temperature sensor through infrared excited blue upconversion emission in Tm3+/Yb3+ codoped Y2O3, Opt Commun. 285 (2012) 1925–1928, https://doi.org/10.1016/j.optcom.2011.12.075.
[43] M. Pollnau, D. Gamelin, S. Lüthi, H. Güdel, M. Hehlen, Power dependence of upconversion luminescence in lanthanide and transition-metal-ion systems, Phys. Rev. B - Condens. Matter Mater. Phys. 61 (2000) 3337–3346, https://doi.org/10.1103/PhysRevB.61.3337.
[44] G. Chen, R. Lei, H. Wang, F. Huang, S. Zhao, S. Xu, Temperature-dependent emission color and temperature sensing behavior in Tm3+/Yb3+:Y2O3 nanoparticles, Opt. Mater. 77 (2018) 233–239, https://doi.org/10.1016/j.optmat.2018.01.039.
[45] M.M. Upadhyay, N.K. Mishra, K. Kumar, Upconversion luminescence based temperature sensing properties and anti-counterfeiting applications of GdNbO4:Tm3+/Yb3+ phosphor, Spectrochim. Acta Part A Mol. Biomol. Spectrosc. 304 (2024) 123333, https://doi.org/10.1016/j.saa.2023.123333.
[46] M. Vega, I.R. Martin, E. Cortés-Adasme, J. Llanos, Enhanced red up-conversion emission in Er3+/Yb3+ co-doped SrSnO3 for optical temperature sensing based on thermally and non-thermally coupled levels, J. Lumin. 244 (2022) 118687, https://doi.org/10.1016/j.jlumin.2021.118687.
[47] Y. Zhuang, D. Wang, Z. Yang, Upconversion luminescence and optical thermometry based on non-thermally-coupled levels of Ca9Y(PO4)7: Tm3+, Yb3+ phosphor, Opt. Mater. 126 (2022) 112167, https://doi.org/10.1016/j.optmat.2022.112167.
[48] H. Song, C. Wang, Q. Han, X. Tang, W. Yan, Y. Chen, J. Jiang, T. Liu, Highly sensitive Tm3+/Yb3+ codoped SrWO4 for optical thermometry, Sensors Actuators A Phys. 271 (2018) 278–282, https://doi.org/10.1016/j.sna.2018.01.037.
[49] N. Rakov, Tm3+,Yb3+: Y2SiO5 up-conversion phosphors: exploration of temperature sensing performance by monitoring the luminescence emission, Phys. B Condens. Matter 628 (2022) 413572, https://doi.org/10.1016/j.physb.2021.413572.
[50] H. Suo, F. Hu, X. Zhao, Z. Zhang, T. Li, C. Duan, M. Yin, C. Guo, All-in-one thermometer-heater up-converting platform YF 3 :Yb 3+ ,Tm 3+ operating in the first biological window, J. Mater. Chem. C 5 (2017) 1501–1507, https://doi.org/10.1039/C6TC05449H.
[51] J.Y. Park, J.W. Chung, H.K. Yang, Versatile fluorescent Gd2MoO6:Eu3+ nanophosphor for latent fingerprints and anti-counterfeiting applications, Ceram. Int. 45 (2019) 11591–11599, https://doi.org/10.1016/j.ceramint.2019.03.030.